

Collider signatures of mirror fermions in the framework of a left-right mirror modelShreyashi Chakdar,^{1,*} Kirtiman Ghosh,^{1,†} S. Nandi,^{1,‡} and Santosh Kumar Rai^{2,§}¹*Department of Physics and Oklahoma Center for High Energy Physics, Oklahoma State University, Stillwater, Oklahoma 74078-3072, USA*²*Regional Centre for Accelerator-based Particle Physics, Harish-Chandra Research Institute, Chhatnag Road, Jhusi, Allahabad 211019, India*

(Received 30 May 2013; published 11 November 2013)

The idea of left-right symmetry with mirror fermions is very appealing from the symmetry point of view. In this picture, unlike the Standard Model, the symmetry is not only left-right symmetric, but each left-handed fermion multiplet is accompanied by a new right-handed fermion multiplet of opposite chirality. In this work, we consider a gauge symmetry, $SU(3)_c \otimes SU(2)_L \otimes SU(2)_R \otimes U(1)_Y$, supplemented by a discrete Z_2 symmetry. Instead of having right-handed multiplets for each left-handed multiplet of the same fermions as in the usual left-right model, the mirror model includes right-handed doublets involving new fermions (called mirrors), and similarly for each right-handed singlet, there are corresponding mirror singlets. Thus the gauge anomaly is naturally absent in this model, and the model also provides a solution for the strong CP problem because of parity conservation. The first stage of symmetry breaking is achieved by a doublet mirror Higgs with a vacuum expectation value $\approx 10^7$ GeV, needed to explain the neutrino mass $\approx 10^{-11}$ GeV. The mirror fermions can mix with the ordinary fermions via a scalar that is singlet under the gauge symmetry. In this model, only light mirror particles, having masses in the few hundred GeV range, are \hat{e} , \hat{u} , \hat{d} with well-defined spectrum. \hat{u} and \hat{d} can be pair produced at the LHC and can be detected as (uZ) and (dZ) resonances. We discuss the signals of these mirror fermions at the LHC and find that the reach at the LHC can be as large as $m_{\hat{q}} \approx 800$ GeV.

DOI: [10.1103/PhysRevD.88.095005](https://doi.org/10.1103/PhysRevD.88.095005)

PACS numbers: 12.60.-i, 12.15.Ff, 14.65.Jk

I. INTRODUCTION

The nonconservation of parity P (the left-right asymmetry of elementary particles) is well incorporated in the Standard Model (SM) of particle physics. However, it has been considered as an unpleasant feature of the model. One possible way to understand the left-right asymmetry of elementary particles is to enlarge the SM into a left-right (LR) symmetric structure and then, by some spontaneously breaking mechanism, recover the SM symmetry structure. For instance, in left-right symmetric models [1], $SU(2)_R$ interactions are introduced to maintain parity invariance at high-energy scales. The symmetry group $SU(2)_L \otimes SU(2)_R \otimes U(1)_{B-L}$ of LR symmetric models can be a part of a grand unified symmetry group such as $SO(10)$ [2] or E_6 [3] or superstring inspired models [4]. In the framework of LR symmetric SM, the SM left-handed fermions are placed in the $SU(2)_L$ doublets as they are in the SM, while the SM right-handed fermions (with the addition of right-handed neutrinos for the case of leptons) are placed in the $SU(2)_R$ doublets. Subsequently, the LR symmetry is spontaneously broken down to the SM electroweak symmetry using suitable Higgs representations.

There are different variants of LR symmetric models that have been proposed in the literature [5–8].

Another interesting solution to the nonconservation of parity in the SM was proposed in a classic paper [9] by Lee and Yang. They postulated the existence of additional (mirror) fermions of opposite chirality to the SM ones to make the world left-right symmetric at high energies. The advantages of models with mirror fermions to solve some problems in particle physics have already been discussed in the literature. For instance, the existence of mirror neutrinos can naturally explain the smallness of neutrino mass via a seesawlike mechanism [10–12]. Moreover, it can also be useful for the dark matter problem [12] and neutrino oscillations, as well as different neutrino physics anomalies such as solar neutrino deficit and atmospheric neutrino anomaly [11]. On the other hand, mirror fermions can provide a solution to the strong CP problem if the parity symmetry is imposed [13,14]. Finally, the existence of mirror particles appears naturally in many extensions of the SM, like grand unified theory (GUT) and string theories [15]. The masses of these mirror particles, though unknown, are not experimentally excluded to be at or below the TeV scale. The agreement of the models with mirror fermions with electroweak precision data, Higgs rate, etc. have been studied in Ref. [16]. Therefore, it is important to study the phenomenological consequences of the mirror particles in the context of collider experiments, in particular at the Large Hadron Collider (LHC). In this paper, we

*chakdar@okstate.edu

†kirti.gh@gmail.com

‡s.nandi@okstate.edu

§skrai@hri.res.in

have investigated the phenomenology of mirror particles in the context of a particular variant of the LR symmetric mirror model (LRMM), their associated final state signals, and the discovery potential at the LHC.

In the LRMM we propose in this work, the SM gauge group ($G_{\text{SM}} = SU(3)_C \otimes SU(2)_L \otimes U(1)_Y$) is extended to $G_{\text{LR}} = SU(3)_C \otimes SU(2)_L \otimes SU(2)_R \otimes U(1)_{Y'}$, together with a discrete Z_2 symmetry. The SM particle spectrum is also extended to include mirror particles and a real scalar Higgs singlet under both $SU(2)_L$ and $SU(2)_R$. For the fermion sector, the right-handed (left-handed) components of mirror fermions transform as doublets (singlets) under $SU(2)_R$. The SM fermions are singlets under $SU(2)_R$, but doublets under $SU(2)_L$. Similarly there are mirror singlet fermions corresponding to the SM singlet fermions. Since the fermion representations are exactly mirror symmetric, all triangle anomalies are exactly canceled with respect to the entire gauge symmetry; the model is anomaly free. Because of even numbers of doublets, there is also no gravitational anomaly. The SM fermions are even under the Z_2 symmetry, whereas the corresponding mirror fermions are odd. Therefore, any mass mixing between SM charged fermions and with mirror partners is forbidden by the Z_2 symmetry. The spontaneous symmetry breaking (SSB), $G_{\text{LR}} \rightarrow G_{\text{SM}}$, is realized by introducing a mirror Higgs doublet that is singlet under $SU(2)_L$ and doublet under $SU(2)_R$. Subsequently the SSB, $G_{\text{SM}} \rightarrow SU(3)_C \otimes U(1)_{\text{EM}}$, is achieved via the SM Higgs doublet, which is doublet under $SU(2)_L$ and singlet under $SU(2)_R$. After the SSB, the gauge boson sector of LRMM contains the usual SM gauge bosons (gluon, W^\pm bosons, Z boson, and photon) along with the mirror partners of W^\pm and Z bosons. The nonzero vacuum expectation value (VEV) for a singlet scalar breaks the Z_2 symmetry and gives rise to mixing between the SM and mirror fermions.

The parity symmetry in LRMM determines the ratio among the charged mirror fermion masses from the SM charged fermion mass spectrum. In particular, the ratio of the SM fermion mass and the corresponding mirror fermion mass is given by $\mathcal{O}(1) \frac{v}{\hat{v}}$, where $\mathcal{O}(1)$ is an order one number, $v \sim 250$ GeV, and \hat{v} are the VEVs for the SM Higgs and mirror Higgs, respectively. Connecting the model for generating tiny neutrino masses $\simeq 10^{-11}$ GeV gives $\hat{v} \sim 10^7$ GeV. This gives TeV scale masses, or a few hundred GeV masses for the mirror partners of electron, up and down quarks, namely \hat{e} , \hat{u} and \hat{d} . This makes the model testable at the ongoing LHC and proposed linear electron-positron collider experiments.

Different variants of LR symmetric mirror models have been proposed and studied in the literature in different contexts. For example, in Ref. [17], the SM particle content has been extended to include mirror fermions, and tiny neutrino mass has been explained via a seesaw mechanism. In this model, the gauge group is the SM gauge group and for each SM left- (right-) handed $SU(2)_L$ doublet (singlet), there is a right- (left-) handed mirror doublet (singlet). Therefore, both

the SM (left-handed) and mirror (right-handed) neutrinos in this model transform as doublets under $SU(2)_L$. As a result, triplet Higgs fields are required in this model for the Majorana mass terms. However, in our model the gauge structure is enlarged, which gives rise to additional heavy gauge bosons, and, in addition to doublet neutrinos, we have singlet left-handed and right-handed neutrinos. Therefore, a similar mirrorlike extension to the SM Higgs sector works and a triplet Higgs is not required in our model. Another class of mirror models has been proposed in Ref. [13] as a solution to the strong CP problem. The gauge group and particle content for our model is somewhat similar to the model in Ref. [13]. However, our model includes a singlet scalar, and the gauge symmetry is supplemented by an additional discrete Z_2 symmetry. These modifications give rise to TeV-scale mirror fermions with phenomenological implications different from other LR symmetric mirror models, testable at the collider experiments.

One of the major goals of the LHC experiment is to find new physics beyond the SM. The LHC is a proton-proton collider, and thus the collision processes are overwhelmed by the QCD interactions. Therefore, in the framework of LRMM, the new TeV-scale colored particles, namely \hat{u} and \hat{d} quarks, will be copiously pair produced at the LHC. After being produced, \hat{u} and \hat{d} quarks will decay to the SM particles giving rise to interesting signatures at the LHC. The TeV-scale mirror quarks are found to decay into a Z or W boson or a Higgs boson in association with a SM quark. This leads to new fermionic resonances as well as new physics signals in two SM gauge bosons + two jet final states. Note that the gauge bosons could be either Z or W , and the highlight of the signal would be the presence of a clear resonance in the jet + Z and jet + W invariant mass distributions. Such a resonance will stand out against any SM background in these final states. In this paper we have therefore studied in detail the signal coming from the pair production of the mirror quarks, \hat{u} and \hat{d} , and their subsequent decays in our LRMM and compared it with the dominant SM background processes.

The paper is organized as follows. In Sec. II we discuss our model and the formalism. Section III is devoted to the phenomenological implications of the model. Finally, a summary of our work and the conclusions are given in Sec. IV.

II. LEFT-RIGHT SYMMETRIC MIRROR MODEL (LRMM) AND THE FORMALISM

Our LR symmetric mirror model is based on the gauge symmetry $G_{\text{LR}} = SU(3)_C \otimes SU(2)_L \otimes SU(2)_R \otimes U(1)_{Y'}$, supplemented by a discrete Z_2 symmetry. Left-right symmetry, as in the usual left-right model, provides a natural explanation of why the parity is violated at low energy. Inclusion of mirror particles gives an alternate realization of the LR symmetry in the fermion sector. The fermion representations in our model for leptons and quarks in the first family is given by

$$\begin{aligned}
l_L^0 &= \begin{pmatrix} \nu^0 \\ e^0 \end{pmatrix}_L \sim (1, 2, 1, -1), & e_R^0 &\sim (1, 1, 1, -2), & \nu_R^0 &\sim (1, 1, 1, 0); \\
\hat{l}_R^0 &= \begin{pmatrix} \hat{\nu}^0 \\ \hat{e}^0 \end{pmatrix}_R \sim (1, 1, 2, -1), & \hat{e}_L^0 &\sim (1, 1, 1, -2), & \hat{\nu}_L^0 &\sim (1, 1, 1, 0); \\
Q_L^0 &= \begin{pmatrix} u^0 \\ d^0 \end{pmatrix}_L \sim \left(3, 2, 1, \frac{1}{3}\right), & u_R^0 &\sim \left(3, 1, 1, \frac{4}{3}\right), & d_R^0 &\sim \left(3, 1, 1, -\frac{2}{3}\right); \\
\hat{Q}_R^0 &= \begin{pmatrix} \hat{u}^0 \\ \hat{d}^0 \end{pmatrix}_R \sim \left(3, 1, 2, \frac{1}{3}\right), & \hat{u}_L^0 &\sim \left(3, 1, 1, \frac{4}{3}\right), & \hat{d}_L^0 &\sim \left(1, 1, 1, -\frac{2}{3}\right).
\end{aligned} \tag{1}$$

where the bracketed entries correspond to the transformation properties under the symmetries of the group G_{LR} . Note that since the model is left-right symmetric, for every fermion representation of $SU(2)_L$, there is a multiplet corresponding to the same representation of $SU(2)_R$. The superscripts (0) denote gauge eigenstates and the hat symbol ($\hat{}$) is associated with the mirror fermions. The charge generator is given by $Q = T_{3L} + T_{3R} + Y'/2$. In the usual LR symmetric model, $SU(2)_L \otimes SU(2)_R \otimes U(1)$, the $U(1)$ symmetry is $U(1)_{B-L}$. This is easily embedded into $SU(4)_C \otimes SU(2)_L \otimes SU(2)_R$ or $SO(10)$ GUT. The $U(1)_{Y'}$ in our model is not $U(1)_{B-L}$. This can be seen from the Y' quantum numbers of the fermions in Eq. (1). Thus $U(1)_{Y'}$, in this model, cannot be embedded in the usual $SO(10)$ GUT.

Under the Z_2 symmetry, the SM fermions as well as the right-handed singlet neutrino (without hat) are even, whereas the mirror fermions including the left-handed singlet mirror neutrino (denoted by hat) are odd. This structure of Z_2 symmetry for the SM and corresponding mirror fermion is required to forbid the large (in general, of the order of symmetry-breaking scale) singlet mass terms between the SM and mirror singlets. The fermion representations for the second and third family are identical to the first family.

Note that in the traditional LR model, the fermion sector is completely symmetric for the ordinary SM fermions. For example, we have $(u, d)_L$ and $(u, d)_R$ and similarly for every fermion family. Another version, proposed in [9], is to introduce new fermions to make it LR symmetric, i.e., for every $(u, d)_L$, we have new fermions, $(\hat{u}, \hat{d})_R$. Hence, it is the left-right mirror model (LRMM). It is this realization that we pursue here. It was shown in Refs. [13,14] that the complete invariance of such a model under parity can guarantee a vanishing strong CP phase from the QCD θ vacuum and thus solve the strong CP problem.

A. Symmetry breaking and the scalar sector

In the framework of LRMM, spontaneous symmetry breaking is achieved via the following steps:

$$SU(2)_L \otimes SU(2)_R \otimes U(1)_{Y'} \rightarrow SU(2)_L \otimes U(1)_Y \rightarrow U(1)_Q. \tag{2}$$

where $Y/2 = T_{3R} + Y'/2$. In order to realize the above SSB, two Higgs doublets are required, i.e., the SM Higgs doublet (Φ) and its mirror partner ($\hat{\Phi}$). Note that in order to generate Dirac mass for the matter fields via Yukawa interactions between doublet and singlet fermions for the SM and mirror sector, both the Higgs doublets have to be even under the Z_2 symmetry. The gauge quantum numbers and VEVs of these Higgs doublets are summarized below:

$$\begin{aligned}
\Phi &\sim (1, 2, 1, 1), & \hat{\Phi} &\sim (1, 1, 2, 1); \\
\langle \Phi \rangle &= \frac{1}{\sqrt{2}} \begin{pmatrix} 0 \\ v \end{pmatrix}, & \langle \hat{\Phi} \rangle &= \frac{1}{\sqrt{2}} \begin{pmatrix} 0 \\ \hat{v} \end{pmatrix}.
\end{aligned} \tag{3}$$

In addition to these two Higgs doublets, we have introduced a singlet (under both $SU(2)_L$ and $SU(2)_R$) real scalar, which is odd under the Z_2 symmetry: $\chi \sim (1, 1, 1, 0)$. The VEV of χ , $\langle \chi \rangle = v_\chi$, breaks the Z_2 symmetry spontaneously. This enables us to generate mixing between the SM fermions and the mirror fermions. This mixing with the SM fermions allows the mirror fermions to decay to lighter SM particles after they are pair produced at colliders such as the LHC, giving rise to interesting final state signals. It is important to mention that spontaneous breaking of Z_2 discrete symmetry gives rise to a domain walls problem in the theory. However, this problem is easily solved by breaking the Z_2 symmetry softly by introducing a $\mu_3 \chi^3$ in the potential. With this soft breaking, the world will have no domain walls, and by choosing μ_3 much smaller than μ_χ , means there will be no significant effect on the mixing and mass terms of the Higgs sector in our model.

In order to generate the above structure of VEVs for Φ and $\hat{\Phi}$, the LR symmetry has to be broken; otherwise, we will end up with $v = \hat{v}$. The most general scalar potential that develops this pattern of VEVs is given by

$$\begin{aligned}
V &= -(\mu^2 \Phi^\dagger \Phi + \hat{\mu}^2 \hat{\Phi}^\dagger \hat{\Phi}) + \frac{\lambda}{2} [(\Phi^\dagger \Phi)^2 + (\hat{\Phi}^\dagger \hat{\Phi})^2] \\
&+ \lambda_1 (\Phi^\dagger \Phi) (\hat{\Phi}^\dagger \hat{\Phi}) - \frac{1}{2} \mu_\chi^2 \chi^2 + \frac{1}{3} \mu_3 \chi^3 \\
&+ \frac{1}{4} \lambda_\chi \chi^4 + \lambda_{\phi\chi} \chi^2 (\Phi^\dagger \Phi + \hat{\Phi}^\dagger \hat{\Phi}).
\end{aligned} \tag{4}$$

It is important to note that in the above potential, the terms with μ , $\hat{\mu}$ break the parity symmetry softly, i.e., only through the dimension-two mass terms of the scalar potential. Note that after the two stages of symmetry breaking, we are left with three neutral scalars, the SM-like Higgs h , the mirror Higgs \hat{h} , and a singlet Higgs χ . We consider a solution of the Higgs potential such that $v \ll v_\chi \ll \hat{v}$, and so the mixing among these Higgses is negligible.

B. Gauge boson masses and mixings

The gauge boson masses and mixings are obtained from the following kinetic terms of the scalars in the Lagrangian:

$$\mathcal{L} \supset (\mathcal{D}_\mu \Phi)^\dagger (\mathcal{D}^\mu \Phi) + (\hat{\mathcal{D}}_\mu \hat{\Phi})^\dagger (\hat{\mathcal{D}}^\mu \hat{\Phi}), \quad (5)$$

where \mathcal{D} and $\hat{\mathcal{D}}$ are the covariant derivatives associated with the SM and mirror sector, respectively.

$$\mathcal{D}_\mu (\hat{\mathcal{D}}_\mu) = \partial_\mu + ig \frac{\tau_a}{2} W_\mu^a (\hat{W}_\mu^a) + ig' \frac{Y'}{2} B_\mu, \quad (6)$$

where λ_a 's and τ_a 's are the Gell-Mann and Pauli matrices, respectively. The gauge bosons and gauge couplings related to the gauge group $SU(2)_L \otimes SU(2)_R \otimes U(1)_{Y'}$ are, respectively, W_μ^a , \hat{W}_μ^a , B_μ , and g , g , g' . Note that to ensure parity symmetry, we have chosen identical gauge couplings for $SU(2)_L$ and $SU(2)_R$.

Substituting the VEVs of Eq. (3) in the kinetic terms for the scalars in Eq. (5), we obtain the masses and mixings of the seven electroweak gauge bosons of this model. The light gauge bosons are denoted by W^\pm , Z and γ , which are identified with the SM ones, whereas the mirror gauge bosons are denoted by \hat{W}^\pm and \hat{Z} . The mass matrix for the charged gauge bosons is diagonal, with masses

$$M_{W^\pm} = \frac{1}{2} g v, \quad M_{\hat{W}^\pm} = \frac{1}{2} g \hat{v}. \quad (7)$$

The mass matrix for the neutral gauge boson sector is not diagonal, and in the basis (W^3, \hat{W}^3, B) , the neutral gauge boson mass matrix is given by

$$M = \frac{1}{4} \begin{pmatrix} g^2 v^2 & 0 & -g g' v^2 \\ 0 & g^2 \hat{v}^2 & -g g' \hat{v}^2 \\ -g g' v^2 & -g g' \hat{v}^2 & g'^2 (v^2 + \hat{v}^2) \end{pmatrix}. \quad (8)$$

This mass matrix can be diagonalized by means of an orthogonal transformation R , which connects the weak eigenstates (W^3, \hat{W}^3, B) to the physical mass eigenstates (Z, \hat{Z}, γ) ,

$$\begin{pmatrix} W^3 \\ \hat{W}^3 \\ B \end{pmatrix} = R \begin{pmatrix} Z \\ \hat{Z} \\ \gamma \end{pmatrix}. \quad (9)$$

We have obtained the eigenvalues and eigenvectors of the matrix in Eq. (8). The eigenvalues correspond to the masses of the physical states. One eigenstate (γ) has zero eigenvalue, which is identified with the SM photon, and the masses of other eigenstates are given by

$$M_Z^2 = \frac{1}{4} v^2 g^2 \frac{g^2 + 2g'^2}{g^2 + g'^2} \left[1 - \frac{g'^4}{(g^2 + g'^2)^2} \epsilon \right], \quad (10)$$

$$M_{\hat{Z}}^2 = \frac{1}{4} \hat{v}^2 (g^2 + g'^2) \left[1 + \frac{g'^4}{(g^2 + g'^2)^2} \epsilon \right],$$

where $\epsilon = v^2/\hat{v}^2$. Since we assume that $\hat{v} \gg v$, the $\mathcal{O}(\epsilon^2)$ terms in Eq. (10) can be neglected. The mixing matrix R in the neutral gauge boson sector can be analytically expressed in terms of the two mixing angles θ_W and $\hat{\theta}_W$. The angles are defined in the following:

$$\cos^2 \theta_W = \left(\frac{M_W^2}{M_Z^2} \right)_{\epsilon=0} = \frac{g^2 + g'^2}{g^2 + 2g'^2}, \quad (11)$$

$$\cos^2 \hat{\theta}_W = \left(\frac{M_{\hat{W}}^2}{M_{\hat{Z}}^2} \right)_{\epsilon=0} = \frac{g^2}{g^2 + g'^2}.$$

The analytic expression for the mixing matrix up to $\mathcal{O}(\epsilon)$ is given by

$$R = \begin{pmatrix} -\cos \theta_W & -\cos \hat{\theta}_W \sin^2 \hat{\theta}_W \epsilon & \sin \theta_W \\ \sin \theta_W \sin \hat{\theta}_W \left[1 + \frac{\cos^2 \hat{\theta}_W}{\cos^2 \theta_W} \epsilon \right] & -\cos \hat{\theta}_W [1 - \sin^4 \hat{\theta}_W \epsilon] & \sin \theta_W \\ \sin \theta_W \cos \hat{\theta}_W \left[1 - \frac{\sin^2 \hat{\theta}_W}{\cos \theta_W} \epsilon \right] & \sin \hat{\theta}_W [1 + \sin^2 \hat{\theta}_W \cos^2 \hat{\theta}_W \epsilon] & \cos \theta_W \cos \hat{\theta}_W \end{pmatrix}. \quad (12)$$

It is important to note that in the limit $\epsilon = 0$, one recovers the SM gauge boson couplings. The couplings of our theory are related to the electric charge (e) by

$$g = \frac{e}{\sin \theta_W}, \quad g' = \frac{e}{\cos \theta_W \cos \hat{\theta}_W}, \quad \text{which implies } \frac{1}{e^2} = \frac{2}{g^2} + \frac{1}{g'^2}. \quad (13)$$

Note that there are only two independent gauge couplings in the theory, which we express in terms of e and $\cos \theta_W$, and therefore $\hat{\theta}_W$ is not an independent angle but is related to θ_W as $\sin \hat{\theta}_W = \tan \theta_W$.

C. Fermion mass and mixing

1. Charged fermion sector

The charged fermion mass Lagrangian includes Yukawa terms for the SM fermions and its mirror partners. Mass terms between the singlet SM fermions and mirror fermions are forbidden by the Z_2 symmetry. However, the Yukawa interactions between the singlet SM fermions and mirror fermions with the singlet scalar χ are allowed. The Lagrangian invariant under our gauge symmetry as well as the Z_2 symmetry for the down-type quark and its mirror partner are given by

$$\begin{aligned} \mathcal{L} \supset & y_d (\bar{Q}_L^0 \Phi d_R^0 + \bar{Q}_R^0 \hat{\Phi} \hat{d}_L^0) + h_d \chi \bar{d}_R \hat{d}_L + \text{H.c.} \\ & \supset \begin{pmatrix} \bar{d}_L^0 & \bar{d}_L^0 \end{pmatrix} \begin{pmatrix} \frac{y_d v}{\sqrt{2}} & 0 \\ M_{d\hat{d}}^* & \frac{y_d^* \hat{v}}{\sqrt{2}} \end{pmatrix} \begin{pmatrix} d_R^0 \\ \hat{d}_R^0 \end{pmatrix} + \text{H.c.}, \end{aligned} \quad (14)$$

where, y_d and h_d are the Yukawa couplings for the SM d quark and $M_{d\hat{d}} = h_d v \chi$. It is important to mention that h_d , in general, is a 3×3 matrix for three families and gives rise to flavor mixing. Flavor mixing in the leptonic sector results in lepton flavor violating (LFV) processes like $\mu \rightarrow e\gamma$, $\tau \rightarrow \mu\gamma$, $\mu \rightarrow eee$, which are highly constrained from *BABAR* [18] and *Belle* [19] experiments. For example, in the present model, the dominant contribution to the flavor violating μ or τ decay arises from the diagram with singlet scalar (χ) and mirror lepton propagating in the loop. LFV processes in the context of models with TeV-scale mirror fermions have already been studied in Ref. [20].

To ensure LR symmetry, we have used the same Yukawa coupling for the ordinary and the mirror sector. Notice that the Yukawa terms involving χ introduce mixing between SM and mirror fermions. The charged fermion mass can be diagonalized via bi-unitary transformation by introducing two mixing angles. The charged fermion mass (physical) eigenstates are related to the gauge eigenstates by the following relation:

$$\begin{pmatrix} f^0 \\ \hat{f}^0 \end{pmatrix}_{L,R} = \begin{pmatrix} \cos \theta^f & \sin \theta^f \\ -\sin \theta^f & \cos \theta^f \end{pmatrix} \begin{pmatrix} f \\ \hat{f} \end{pmatrix}_{L,R}, \quad (15)$$

where $f_{L,R}$ can be identified with the left- and right-handed components of the SM fermions and $\hat{f}_{L,R}$ corresponds to the heavy mirror fermions. The masses and mixing angles are given by

$$\begin{aligned} m_f &= \frac{y_f v}{\sqrt{2}}, & m_{\hat{f}} &= \sqrt{\frac{y_f^2 \hat{v}^2 + 2M_{f\hat{f}}^2}{2}}, \\ \tan 2\theta_R^f &= \frac{2\sqrt{2}y_f M_{f\hat{f}} \hat{v}}{y_f^2(v^2 - \hat{v}^2) + 2M_{f\hat{f}}^2}, \\ \tan 2\theta_L^f &= \frac{2\sqrt{2}y_f M_{f\hat{f}} v}{y_f^2(v^2 - \hat{v}^2) - 2M_{f\hat{f}}^2}. \end{aligned} \quad (16)$$

2. Neutrino sector

Under the Z_2 symmetry, the singlet right-handed neutrinos are even, and singlet left-handed neutrinos are odd. Therefore, the mass terms between the left-handed and right-handed singlet neutrinos are not allowed. Since the singlet scalar field χ is odd under the Z_2 symmetry, Yukawa terms involving the singlet neutrinos and χ are allowed. The Lagrangian allowed by our gauge symmetry and respecting the discrete Z_2 symmetry is given by

$$\begin{aligned} \mathcal{L} \supset & f_\nu (\bar{l}_L^0 \Phi \nu_R^0 + \bar{l}_R^0 \hat{\Phi} \hat{\nu}_L^0) + M \nu_R^{0T} C^{-1} \nu_R^0 + h_\nu \chi \bar{\nu}_R^0 \hat{\nu}_L^0 \\ & + M \hat{\nu}_L^{0T} C^{-1} \hat{\nu}_L^0 + \text{H.c.}, \end{aligned}$$

where f_ν is the neutrino Yukawa coupling, and M is the singlet neutrino mass of order \hat{v} . The neutrino mass matrix with both Dirac mass ($m = f_\nu v/\sqrt{2}$, $m' = f_\nu \hat{v}/\sqrt{2}$ and $M_{\nu\hat{\nu}} = h_\nu v \chi$) and Majorana mass (M)¹ terms in the $(\nu_L^0, \nu_R^0, \hat{\nu}_R^0, \hat{\nu}_L^0)$ basis is given by

$$\begin{pmatrix} 0 & m & 0 & 0 \\ m & M & 0 & M_{\nu\hat{\nu}} \\ 0 & 0 & 0 & m' \\ 0 & M_{\nu\hat{\nu}} & m' & M \end{pmatrix}. \quad (17)$$

Assuming $M_{\nu\hat{\nu}} \sim M$, the orders of magnitude for the eigenvalues of the neutrino mass matrix are

$$-m^2/M, \quad m'/\sqrt{2}, \quad -m'/\sqrt{2}, \quad 2M. \quad (18)$$

Thus, to generate a light neutrino mass $\simeq 10^{-11}$ GeV with a Yukawa coupling strength of $f_\nu \sim 10^{-4(6)}$ (which is somewhat similar to the Yukawa coupling of the electron), we need $\hat{v} \sim 10^{7(3)}$ GeV. This $\hat{v} \sim 10^{7(3)}$ scale and $M_{f\hat{f}}$ [see Eq. (16)] determines the masses of the mirror fermions. For the first family, the mirror fermion masses then come out to be in the range of a few hundred GeV to a few TeV. Note that fitting the neutrino mass and mixing angles to experimental data would require a more detailed analysis of the neutrino sector, which we leave for future studies. Another realization with a mirrorlike symmetry to generate neutrino masses was considered in Ref. [17].

III. PHENOMENOLOGY

In this section, we discuss the collider phenomenology of the LRMM. Before going into the details of the collider signatures of LRMM, we first need to study the properties of mirror fermions and bosons. From the point of view of collider phenomenology, we are interested in the interactions between SM particles and mirror particles, which give the production and decay properties of the mirror

¹Note that it is not necessary to have the same Majorana mass terms for the SM and mirror singlet neutrinos. Here, $M \sim \hat{v}$ represents the order of magnitude of the Majorana mass terms.

particles. The Lagrangian for the charge currents with W^\pm and \hat{W}^\pm boson contributions is given by,

$$\mathcal{L}_{\text{CC}} = -\frac{g}{2\sqrt{2}}\bar{f}\gamma^\mu[A_{ff'}^W(1-\gamma^5)W_\mu^- + A_{ff'}^{\hat{W}}(1+\gamma^5)\hat{W}_\mu^-]f', \quad (19)$$

where the coefficients $A_{ff'}^W$ and $A_{ff'}^{\hat{W}}$ depend on the charged fermion mixing angles θ_L and θ_R . The analytical expressions for these coefficients are presented in Table I² for up- and down-flavored SM and mirror fermions. The neutral current interactions of fermions with neutral gauge bosons (γ , Z and \hat{Z} bosons) are described by the following Lagrangian:

$$\begin{aligned} \mathcal{L}_{\text{NC}} = & -eQ_f\bar{f}\gamma^\mu A_\mu f \\ & -\frac{1}{6}\frac{g}{\cos^3\theta_W}\bar{f}\gamma^\mu\left[A_{ff'}^Z\frac{1-\gamma^5}{2} + B_{ff'}^Z\frac{1+\gamma^5}{2}\right]Z_\mu f' \\ & -\frac{1}{6}\frac{g}{\cos^3\theta_W\sqrt{\cos 2\theta_W}}\bar{f}\gamma^\mu \\ & \times\left[A_{ff'}^{\hat{Z}}\frac{1-\gamma^5}{2} + B_{ff'}^{\hat{Z}}\frac{1+\gamma^5}{2}\right]\hat{Z}_\mu f', \end{aligned} \quad (20)$$

where e is electron charge and Q_f is the charge of fermion f . For up- and down-flavored SM and mirror fermions, analytical expressions up to $O(\epsilon)$ for the coefficients $A_{ff'}^Z$, $B_{ff'}^Z$ are presented in Table II. The interactions of fermions with the SM Higgs and mirror Higgs are described in Eq. (21),

TABLE I. Analytical expressions for $A_{ff'}^W$ and $A_{ff'}^{\hat{W}}$. Note that we have assumed $V_{ud} = 1$. We have also assumed fermion mixing angles (θ_L and θ_R) are the same for up and down flavor.

f	f'	$A_{ff'}^W$	$A_{ff'}^{\hat{W}}$
d	u	$\cos^2\theta_L$	$\sin^2\theta_R$
d	\hat{u}	$\cos\theta_L\sin\theta_L$	$-\cos\theta_R\sin\theta_R$
\hat{d}	u	$\cos\theta_L\sin\theta_L$	$-\cos\theta_R\sin\theta_R$
\hat{d}	\hat{u}	$\sin^2\theta_L$	$\cos^2\theta_R$

$$\begin{aligned} \mathcal{L}_S = & \frac{y_f}{\sqrt{2}}\bar{f}\left[A_{ff'}^H\frac{1-\gamma^5}{2} + B_{ff'}^H\frac{1+\gamma^5}{2}\right]Hf'\frac{y_f}{\sqrt{2}}\bar{f} \\ & \times\left[A_{ff'}^{\hat{H}}\frac{1-\gamma^5}{2} + B_{ff'}^{\hat{H}}\frac{1+\gamma^5}{2}\right]\hat{H}f', \end{aligned} \quad (21)$$

where y_f is the Yukawa coupling of fermion f . The expressions for the coefficients $A_{ff'}^H$, $B_{ff'}^H$, $A_{ff'}^{\hat{H}}$ and $B_{ff'}^{\hat{H}}$ can be found in Table III. It is important to note that in the limit $\epsilon = 0$ and $\cos\theta_{L,R} = 1$, the SM fermions decouple from the mirror fermions and we recover the SM couplings.

The decays of the TeV-scale mirror fermions into \hat{W} , \hat{Z} or \hat{H} are kinematically forbidden since the mass of these mirror bosons is proportional to $\hat{v} \sim 10^7$ GeV. Because of the mixing of the mirror fermions with the ordinary fermions, the mirror fermions can decay into a SM fermion, and a Z , W or a Higgs boson. The expressions for the partial decay widths are

$$\begin{aligned} \Gamma(\hat{f} \rightarrow fZ) &= \frac{g^2}{36\cos^6\theta_W} \frac{(A_{ff'}^Z)^2 + (B_{ff'}^Z)^2}{64\pi} \frac{M_{\hat{f}}^3}{M_Z^2} \left(1 - \frac{M_Z^2}{M_{\hat{f}}^2}\right)^2 \left(1 + 2\frac{M_Z^2}{M_{\hat{f}}^2}\right), \\ \Gamma(\hat{f} \rightarrow f'W) &= \frac{g^2}{8} \frac{(A_{ff'}^W)^2 + (B_{ff'}^W)^2}{16\pi} \frac{M_{\hat{f}}^3}{M_W^2} \left(1 - \frac{M_W^2}{M_{\hat{f}}^2}\right)^2 \left(1 + 2\frac{M_W^2}{M_{\hat{f}}^2}\right), \\ \Gamma(\hat{f} \rightarrow fH) &= \frac{y_f^2}{2} \frac{(A_{ff'}^H)^2 + (B_{ff'}^H)^2}{64\pi} M_{\hat{f}} \left(1 - \frac{M_H^2}{M_{\hat{f}}^2}\right)^2, \end{aligned} \quad (22)$$

where, M_Z , M_W , M_H and $M_{\hat{f}}$ are the masses of the Z , W , Higgs and mirror fermions, respectively. Apart from the known SM parameters and mirror fermion masses, the decay widths of mirror fermions depend on ϵ , θ_L and θ_R . For $\hat{v} \sim 10^7$ GeV, the value of ϵ is about 10^{-10} . Therefore, the terms proportional to ϵ in the decay widths can be safely neglected. The mirror fermions' decay widths depend primarily on the fermion mixing angles. According to Eq. (16), the fermion mixing angles are determined in

²Fermion mixing angles (θ_L and θ_R) depend on the Yukawa coupling of the corresponding fermion. Therefore, the mixing angles are different for up and down flavor. However, we have used the same symbol for the mixing angles of up and down quarks.

terms of two parameters, namely \hat{v} and $M_{f\hat{f}}$. Assuming the up-quark Yukawa coupling, $y_u = 1.3 \times 10^{-5}$, and the SM VEV, $v = 250$ GeV, in Fig. 1, we show the mixing angles, $\sin\theta_L$ (left panel) and $\sin\theta_R$ (right panel), by color gradient in the \hat{v} - $M_{f\hat{f}}$ plane. Equation (16) shows that $\tan 2\theta_L$ is suppressed by the SM quark mass ($\sim y_f v$) in the numerator and by the mirror quark mass ($\sim \sqrt{y_f^2 \hat{v}^2 + 2M_{f\hat{f}}^2}$) in the denominator. Therefore, for a MeV-scale SM quark and a TeV-scale mirror partner, the value of $\sin\theta_L$ is about 10^{-6} , which can be seen in Fig. 1 (left panel). Whereas Fig. 1 (right panel) shows that $\sin\theta_R$ can be large depending on the values of \hat{v} and $M_{f\hat{f}}$.

TABLE II. Analytical expressions for $A_{ff'}^Z$ and $B_{ff'}^Z$.

f	f'	$A_{ff'}^Z$	$B_{ff'}^Z$
d	d	$3\cos^2\theta_L\cos^2\theta_W - 2\cos^2\theta_W\sin^2\theta_W$ $-(1 - 3\sin^2\theta_L)\sin^2\theta_W\epsilon$	$-2\cos^2\theta_W\sin^2\theta_W - 3\sin^2\theta_R\sin^2\theta_W\sqrt{\cos 2\theta_W}\epsilon$ $+(2 - 3\sin^2\theta_R)\sin^3\theta_W\epsilon$
d	\hat{d}	$3\cos^2\theta_W\sin\theta_L\cos\theta_L - 3\sin\theta_L\sin^3\theta_W\cos\theta_L\epsilon$	$3\sin\theta_R\sin^2\theta_W\cos\theta_R\sqrt{\cos 2\theta_W}\epsilon$ $+3\sin\theta_R\sin^3\theta_W\cos\theta_R\epsilon$
\hat{d}	\hat{d}	$3\cos^2\theta_W\sin^2\theta_L - 2\cos^2\theta_W\sin^2\theta_W$ $+(2 - 3\sin^2\theta_L)\sin^3\theta_W\epsilon$	$-3\cos^2\theta_R\sin^2\theta_W\sqrt{\cos 2\theta_W}\epsilon$ $-(1 - 3\sin^2\theta_R)\sin^3\theta_W\epsilon$
u	u	$-3\cos^2\theta_L\cos^2\theta_W + 4\cos^2\theta_W\sin^2\theta_W$ $-(1 + 3\sin^2\theta_L)\sin^3\theta_W\epsilon$	$+4\cos^2\theta_W\sin^2\theta_W + 3\sin^2\theta_R\sin^2\theta_W\sqrt{\cos 2\theta_W}\epsilon$ $-(4 - 3\sin^2\theta_R)\sin^3\theta_W\epsilon$
u	\hat{u}	$-3\cos^2\theta_W\sin\theta_L\cos\theta_L + 3\sin\theta_L\sin^3\theta_W\cos\theta_L\epsilon$	$-3\sin\theta_R\sin^2\theta_W\cos\theta_R\sqrt{\cos 2\theta_W}\epsilon$ $-3\sin\theta_R\sin^3\theta_W\cos\theta_R\epsilon$
\hat{u}	\hat{u}	$-3\cos^2\theta_W\sin^2\theta_L + 4\cos^2\theta_W\sin^2\theta_W$ $-(4 - 3\sin^2\theta_L)\sin^3\theta_W\epsilon$	$4\cos^2\theta_W\sin^2\theta_W + 3\cos^2\theta_R\sin^2\theta_W\sqrt{\cos 2\theta_W}\epsilon$ $-(1 + 3\sin^2\theta_R)\sin^3\theta_W\epsilon$

TABLE III. Analytical expressions for $A_{ff'}^H$, $B_{ff'}^H$, $A_{ff'}^{\hat{H}}$ and $B_{ff'}^{\hat{H}}$.

f	f'	$A_{ff'}^H$	$B_{ff'}^H$	$A_{ff'}^{\hat{H}}$	$B_{ff'}^{\hat{H}}$
f	f	$\cos\theta_L\cos\theta_R$	$\cos\theta_L\cos\theta_R$	$\sin\theta_L\sin\theta_R$	$\sin\theta_L\sin\theta_R$
f	\hat{f}	$\sin\theta_L\cos\theta_R$	$\cos\theta_L\sin\theta_R$	$-\cos\theta_L\sin\theta_R$	$-\sin\theta_L\cos\theta_R$
\hat{f}	\hat{f}	$\sin\theta_L\sin\theta_R$	$\sin\theta_L\sin\theta_R$	$\cos\theta_L\cos\theta_R$	$\cos\theta_L\cos\theta_R$

The neutral [see Eq. (20)] and charge [see Eq. (19)] current interactions of mirror quarks with SM quarks and Z or W bosons are suppressed by $\sin\theta_L$. Moreover, the interactions of mirror quarks with the SM quarks and

Higgs boson are suppressed by the Yukawa couplings. Therefore, before going into the details of collider analysis, it is important to ensure that light mirror quarks decay inside the detectors of the LHC experiment. In Fig. 2, we plot the total decay width of the up-type mirror quark as a function of $\sin\theta_R$ for three different values of the mirror quark mass, viz., $M_{\hat{u}} = 300, 500$ and 1000 GeV. We have considered the lowest possible value of $\sin\theta_L = 10^{-6}$ in Fig. 2. According to Fig. 2, the total decay width of the up-type mirror quark is always greater than 10^{-12} GeV, $\Gamma_{\text{total}} > 10^{-12}$ GeV, which corresponds to a mean distance of $c\tau < 10^{-3}$ cm (without including Lorentz boost)

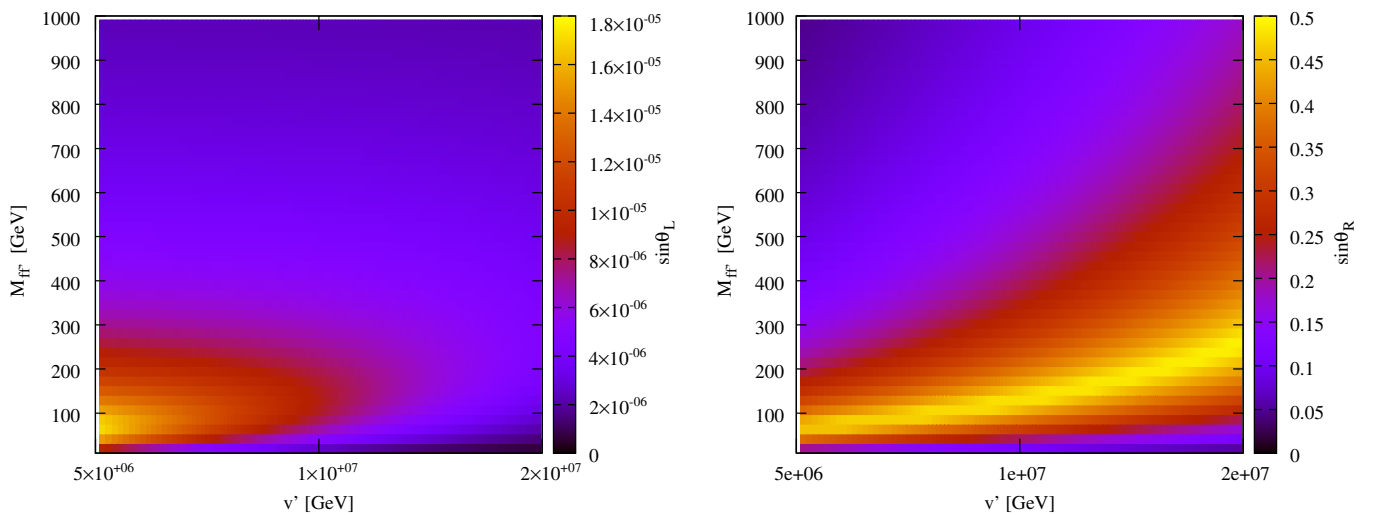


FIG. 1 (color online). Fermion mixing angles, $\sin\theta_L$ (left panel) and $\sin\theta_R$ (right panel), for the up quark are presented by color gradient on the LRMM parameter space defined by \hat{v} (along the x axis) and $M_{\hat{f}\hat{f}}$ (along the y axis). The up-quark Yukawa coupling, $y_u = 1.3 \times 10^{-5}$, and the SM VEV, $v = 250$ GeV, are assumed in these plots.

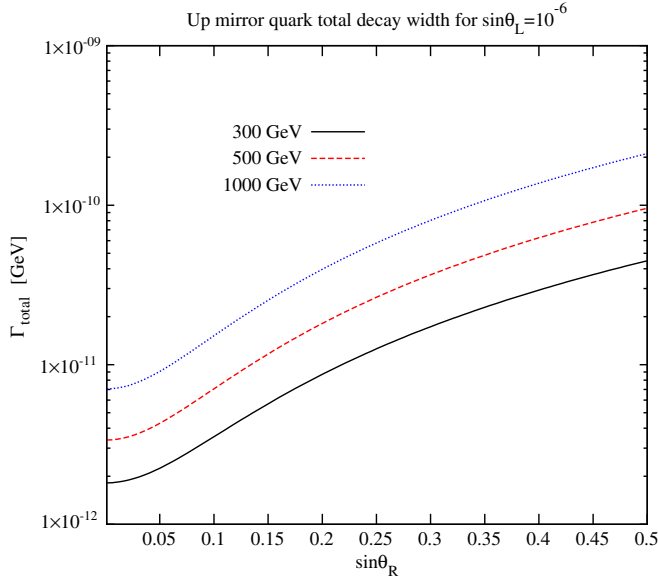


FIG. 2 (color online). Total decay width of up-type mirror quark for three different values of $M_{\hat{u}} = 300, 500$ and 1000 GeV as a function of $\sin \theta_R$. We have assumed the lowest possible value for $\sin \theta_L = 10^{-6}$ in this plot.

traversed by a mirror quark inside a detector before its decay. These numbers assure us that the mirror quarks will always decay inside the detector for a wide range of model parameters.

In Fig. 3, we plot the branching ratios for the up-type mirror quark into dW , uZ and uH channel as a function of $\sin \theta_R$. We have assumed two different values of $\sin \theta_L = 10^{-5}$ (left panel) and 10^{-6} (right panel). We have varied the

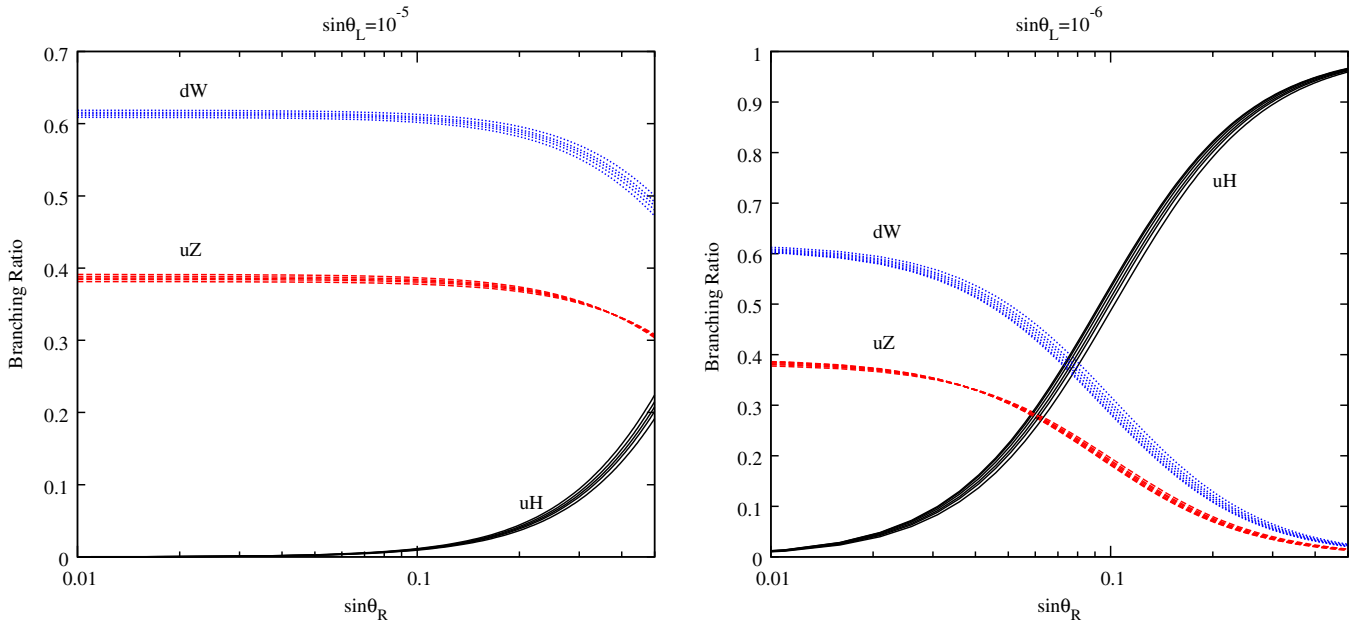


FIG. 3 (color online). Illustrating the up-type mirror quark branching ratios in dW , uZ and uH channel as a function of $\sin \theta_R$ for two different values of $\sin \theta_L = 10^{-5}$ (left panel) and 10^{-6} (right panel). We have varied \hat{u} mass over a range between 300 GeV to 1 TeV which gives rise to the bands instead of lines.

mirror quark mass over 300 GeV to 1 TeV, which gives rise to the bands in Fig. 3. Figure 3 (left panel) shows that for $\sin \theta_L = 10^{-5}$, the decay of \hat{u} into SM vector bosons dominates over the decay into the Higgs boson. Whereas for $\sin \theta_L = 10^{-6}$ (right panel), the decay into vector bosons dominates only in the low- $\sin \theta_R$ region ($\sin \theta_R < 0.08$).

A. Signature of mirror fermions at the LHC

In this section, we will first discuss the production of TeV-scale mirror quarks, namely \hat{u} and \hat{d} quarks, at the LHC. As a consequence of the Z_2 symmetry, the couplings between a mirror quark and the SM particles are forbidden. Therefore, in the presence of this Z_2 symmetry, the single production of the mirror fermions is not possible at the collider. As discussed in the previous section, spontaneous breaking of the Z_2 symmetry introduces mixing between the mirror and SM quarks and thus gives rise to interactions between mirror and SM quarks with a Z , W or Higgs boson. However, the single production rates of TeV-scale mirror quarks via the Z_2 symmetry-violating couplings are suppressed by the quark mixing angles. Therefore, in this work, we have considered the pair production of mirror quarks at the LHC.

As the mirror quarks carry $SU(3)_C$ quantum numbers, they couple directly to the gluons. The pair production of TeV-scale mirror quarks, namely $\hat{u} \hat{u}$ and $\hat{d} \hat{d}$ production, in a proton-proton collision, therefore, is analogous to that of the pair production of SM heavy quarks, the analytic expressions for which can be found in Ref. [21]. Both

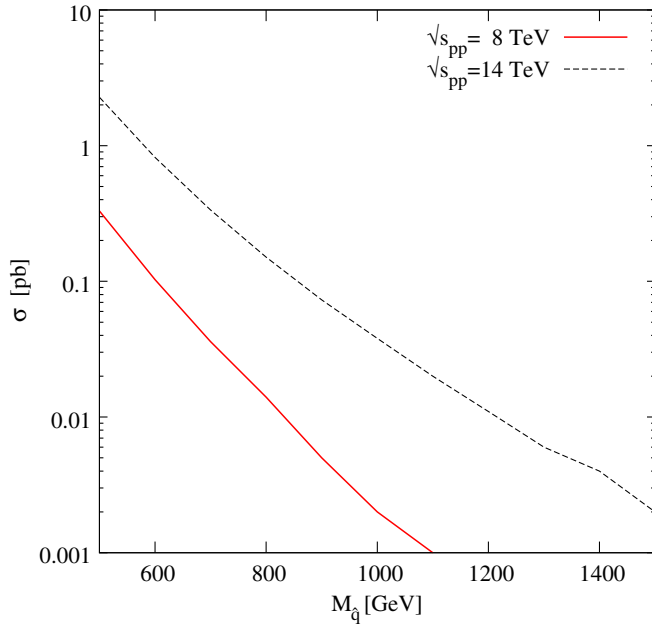


FIG. 4 (color online). Pair production cross sections of mirror quarks as a function of their masses in proton-proton collisions at center-of-mass energies 8 and 14 TeV, respectively.

gluon-gluon (gg) and quark-antiquark ($q\bar{q}$) initial states contribute to the pair production ($\hat{q}\bar{\hat{q}}$) of mirror quarks (see Fig. 5). For numerical evaluation of the cross sections, we have used a tree-level Monte Carlo program incorporating CTEQ6L [22] parton distribution functions. Both the renormalization and the factorization scales have been set equal to the subprocess center-of-mass energy $\sqrt{\hat{s}}$. The ensuing leading-order (LO) $\hat{q}\bar{\hat{q}}$ production cross sections are presented in Fig. 4 as a function of mirror quark mass ($M_{\hat{q}}$) for two different values of the proton-proton center-of-mass energy, viz., $\sqrt{s_{pp}} = 8$ and 14 TeV. While the next-to-leading order and next-to-leading logarithms corrections can be well estimated by a proper rescaling of the corresponding results for $t\bar{t}$ production, we deliberately resist doing so. With the K factor expected to be large [23], our results would thus be a conservative one. The pair production cross section is found to be a few hundred femtobarns (fb) for mirror quark mass of close to 1 TeV. As discussed before, these mirror quarks once produced will decay within the detector. We now analyze the possible signatures of mirror quarks at the LHC following their decay properties. Mirror quarks can decay into a Z boson, a W boson or a Higgs boson in association with a

SM quark: $\hat{q} \rightarrow qZ$, $q'W$ or qH . Thus the pair production of mirror quarks at the LHC gives rise to a pair of heavy SM bosons (Z boson, W boson or Higgs boson) in association with multiple jets in the final state. In this work, we have focused on the signal with the vector bosons in the final states. We choose the LRMM parameter space, where the decay of mirror quarks into vector bosons dominates over decay into the Higgs boson. Figure 3 shows that for the negligible $\hat{q} \rightarrow qH$ branching ratio, the mirror quarks decay into qW and qZ pairs with about 61% and 39% branching probability, respectively. In the rest of our analysis, we have used the above-mentioned values for the decay probability to compute the signal cross sections. Pair production and the decay of mirror quarks into qW and qZ channels give rise to the following signatures:

- (i) 2 jets + 2Z final state arises when both mirror quarks decay into qZ pairs,

$$pp \rightarrow \hat{q}\bar{\hat{q}} \rightarrow (qZ)(\bar{q}Z).$$

The production and decay of mirror quarks in this channel are schematically shown in Fig. 5.

- (ii) 2 jets + Z + W final state results when one mirror quark decays into qZ channel and other one decays into qW channel,

$$pp \rightarrow \hat{q}\bar{\hat{q}} \rightarrow (qZ)(\bar{q}'W).$$

- (iii) If both mirror quarks decay into the qW channel, then pair production of mirror quarks gives rise to a 2 jets + 2W final state.

We consider the reconstruction of mirror quark mass from the invariant mass distribution of qZ pairs, which is possible for the first two signal topologies only. Therefore, we have only considered 2 jets + 2Z and 2 jets + Z + W final states for further analysis. Note that in the leptonic channel, the Z reconstruction would be very clean, while for the 2 jets + Z + W , even the W can be reconstructed well as there is only a single neutrino in the final state. The W 's can be reconstructed in the all-hadronic mode but with significant challenge in efficiencies in a hadronic machine such as the LHC. So we have chosen to neglect the 2 jets + 2W final state in our analysis.

1. 2 jets + 2Z bosons signature

In this section, we have investigated the 2 jets + 2Z final state as a signature of mirror quarks in the framework of LRMM. We have used a parton-level Monte Carlo

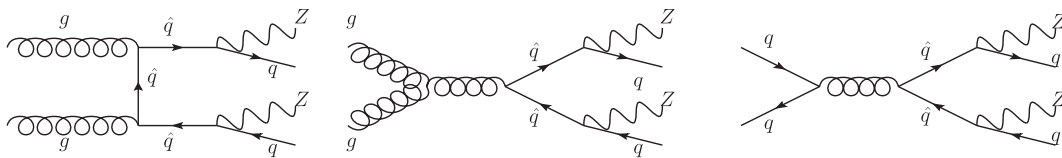


FIG. 5. Feynman diagrams for the $\hat{q}\bar{\hat{q}}$ production and their subsequent decay to qZ .

simulation to evaluate the cross sections and different kinematic distributions for the signal. We have assumed that Z bosons decaying into leptons (electrons and muons) can be identified at the LHC with good efficiency. Therefore, in our parton-level analysis, we consider the Z boson as a standard object³ without simulating its decay to leptons. We must, however, point out that the total number of signal events is crucial in identifying the Z boson in the leptonic channel because of the small branching probability of the Z decaying to charged leptons.

The dominant SM background to the signal comes from the pair production of Z bosons in association with two jets. Before going into the details of signal and background, it is important to list a set of basic requirements for jets to be visible at the detector. To parametrize detector acceptance and enhance signal-to-background ratio, we have imposed kinematic cuts (acceptance cuts), listed in Table IV, on the jets (denoted by j_1 and j_2) after ordering the jets according to their transverse momentum (p_T) hardness ($p_T^{j_1} > p_T^{j_2}$). It should also be realized that any detector has only a finite resolution. For a realistic detector, this applies to both energy and transverse momentum measurements as well as to determination of the angle of motion. For our purpose, the latter can be safely neglected,⁴ and we simulate the former by smearing the jet energy with Gaussian functions defined by an energy-dependent width, σ_E ,

$$\frac{\sigma_E}{E} = \frac{0.80}{\sqrt{E}} \oplus 0.05, \quad (23)$$

where \oplus denotes a sum in quadrature.

The signal jets arise from the decay of a significantly heavy mirror quark to a SM Z and jet. Due to the large phase space available for the decay of the mirror quarks, the resulting jets will be predominantly hard. Therefore, the large jet p_T cuts, listed in Table IV, are mainly aimed at reducing the SM background contributions. With the set of acceptance cuts (see Table IV) and detector resolution defined in the previous paragraph, we compute the signal and background cross sections at the LHC operating with $\sqrt{s} = 8$ and 14 TeV, respectively, and display them in Table V. Table V shows that signal cross sections are larger than the background for lower values of mirror quark masses. However, if we increase $M_{\hat{q}}$, signal cross sections fall sharply as the pair production cross section for the mirror quarks falls with increasing mass.

Since the mirror quarks decay into a jet and Z boson, the signal is characterized by a peak at $M_{\hat{q}}$ in the invariant

³All the cross sections (signal as well as background) presented in the next part of this paper are multiplied by the leptonic branching fraction (6.7% in electron and muon channel) of the Z boson.

⁴The angular resolution is, generically, far superior to the energy/momentum resolutions and too fine to be of any consequence at the level of sophistication of this analysis.

TABLE IV. Acceptance cuts on the kinematical variables. $p_T^{j_{1,2}}$ is the transverse momentum and $\eta^{j_{1,2}}$ is the rapidity of the jets. $\Delta R(j_1, j_2) = \sqrt{(\Delta\eta)^2 + (\Delta\phi)^2}$ is the distance among the jets in the η - ϕ plane, with ϕ being the azimuthal angle.

Kinematic variable	Minimum value	Maximum value
$p_T^{j_{1,2}}$	100 GeV	...
$\eta^{j_{1,2}}$	-2.5	2.5
$\Delta R(j_1, j_2)$	0.7	...

mass distributions of jet- Z pairs. The signal consists of two jets and two Z bosons. In the absence of any knowledge about the right jet- Z pair arising from a particular \hat{q} decay, we have ordered the jets and Z 's according to their p_T hardness ($p_T^{j_1} > p_T^{j_2}$ and $p_T^{Z_1} > p_T^{Z_2}$) and constructed invariant mass distributions in the jet- Z pairs as follows: M_{11} = invariant mass of j_1 and Z_1 ; M_{12} = invariant mass of j_1 and Z_2 ; M_{21} = invariant mass of j_2 and Z_1 ; and M_{22} = invariant mass of j_2 and Z_2 . The four invariant mass distributions (for both signal and the SM background) are presented in Fig. 6 for the LHC with center-of-mass energy 8 (left panel) and 14 TeV (right panel). In Fig. 6, we have presented the signal invariant mass distributions for two different values of $M_{\hat{q}}$. We have included the leptonic branching ratio (6.7% into electron and muon channel) of the Z boson into the cross section in Fig. 6. Figure 6 shows that the signal peaks are clearly visible over the SM background. Moreover, it is important to notice that signal peaks are more prominent in M_{12} and M_{21} distributions compared to M_{11} and M_{22} distributions. Due to the momentum conservation in the transverse direction at the LHC, both the mirror quarks are produced with equal and opposite transverse momentum.⁵ Therefore, if the decay of a particular mirror quark gives rise to the hardest jet, it is more likely that the Z boson arising in the same decay will be the softest one. $M_{12}(M_{21})$ is the invariant mass of hardest-softest (softest-hardest) jet- Z pairs, which come from the decay of a particular \hat{q} in most of the events. As a result, we observe more prominent peaks in the signal $M_{12}(M_{21})$ distribution compared to the $M_{11}(M_{22})$ distribution. In our analysis, we have utilized this feature of the signal for the further enhancement of signal-to-background ratio. Our final event selection criteria (S.C.) is summarized in the following:

- (i) To ensure the observability of a peak for a given luminosity in the signal M_{12} distribution, we have imposed the following criteria: (i) there are at least five signal events in the peak bin and (ii) the number of signal events in the peak bin is greater than the 3σ

⁵We do not consider initial/final state radiation (ISR/FSR) in our analysis. In the presence of ISR/FSR, the transverse momentum of the mirror quarks might not be exactly equal and opposite.

TABLE V. Signal and SM background cross section after the acceptance cuts (A.C.) and selection cuts (S.C.) for two different values of proton-proton center-of-mass energies. Signal cross sections (σ_{Signal}) are presented for three different values of mirror quark masses ($M_{\hat{q}}$).

$\sqrt{s} = 8 \text{ TeV}$					$\sqrt{s} = 14 \text{ TeV}$				
Cross sections (fb)					Cross sections (fb)				
$M_{\hat{q}}$ [GeV]	Signal		Background		$M_{\hat{q}}$ [GeV]	Signal		Background	
	A.C.	S.C.	A.C.	S.C.		A.C.	S.C.	A.C.	S.C.
300	1.65	1.07		0.08	400	2.93	1.5		0.22
350	0.92	0.52	0.35	0.07	500	1.04	0.48	1.36	0.14
400	0.5	0.26		0.05	600	0.40	0.18		0.09

fluctuation of the SM background events in the same bin.

- (ii) If the signal peak in the M_{12} distribution was detectable, then we selected events in the bins corresponding to the peak in the M_{12} distribution and its four (two on the left-hand side and two on the right-hand side) adjacent bins as signal events. We have used a bin size of 20 GeV.
- (iii) The total number of SM background events is given by the sum of events of the above mentioned five bins in the background M_{12} distribution.

After imposing the final event selection criteria, the signal and background cross sections for different $M_{\hat{q}}$ and \sqrt{s} are presented in Table V. Table V shows that selection cuts significantly suppress the SM background cross section, whereas signal cross sections are reduced only by a factor of ~ 2 .

After discussing the characteristic features of the signal and the SM background, we are now equipped to discuss the discovery reach of this scenario at the LHC with center-of-mass energy 8 and 14 TeV. We define the signal to be

observable over the background with confidence level (C.L.) X for an integrated luminosity \mathcal{L} if the X -C.L. upper limit on the background is smaller than the X -C.L. lower limit on the signal plus background [24],

$$\mathcal{L}(\sigma_S + \sigma_B) - N\sqrt{\mathcal{L}(\sigma_S + \sigma_B)} > \mathcal{L}\sigma_B + N\sqrt{\mathcal{L}\sigma_B}, \quad (24)$$

or, equivalently,

$$\sigma_S > \frac{N^2}{\mathcal{L}} \left[1 + 2\frac{\sqrt{\mathcal{L}\sigma_B}}{N} \right], \quad (25)$$

where σ_S and σ_B are the signal and background cross sections, respectively, and $N = 2.5$ for $X = 99.4\%$ [25] C.L. discovery. The signal and background cross sections in Table V show that at the LHC with center-of-mass energy 8 (14 TeV), 350 (550 GeV) mirror quark mass can be probed with integrated luminosity 25 (72 fb^{-1}). In Fig. 7 we have presented the required luminosity for 99.4% C.L. discovery as a function of $M_{\hat{q}}$ for the LHC with center-of-mass energy 8 and 14 TeV.

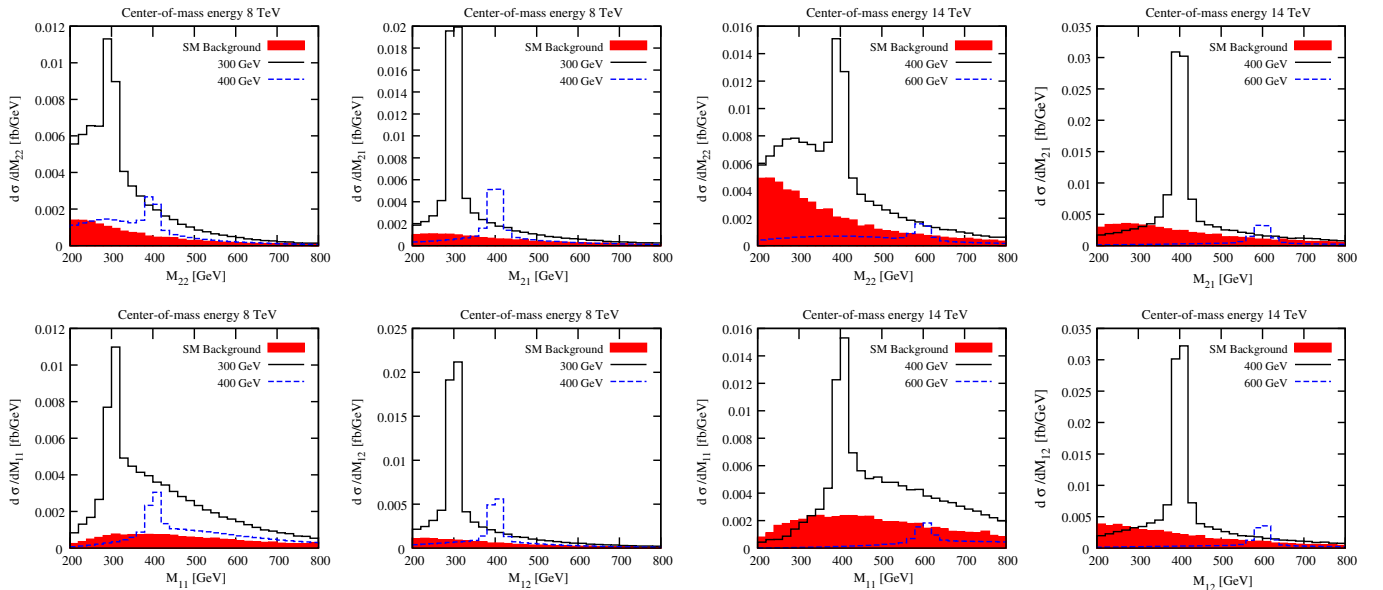


FIG. 6 (color online). Jet-Z invariant mass distributions after ordering the jets ($p_T^1 > p_T^2$) and Z's ($p_T^Z > p_T^{\bar{Z}}$) according to their p_T hardness for the LHC with center-of-mass energy 8 (left panel) and 14 TeV (right panel).

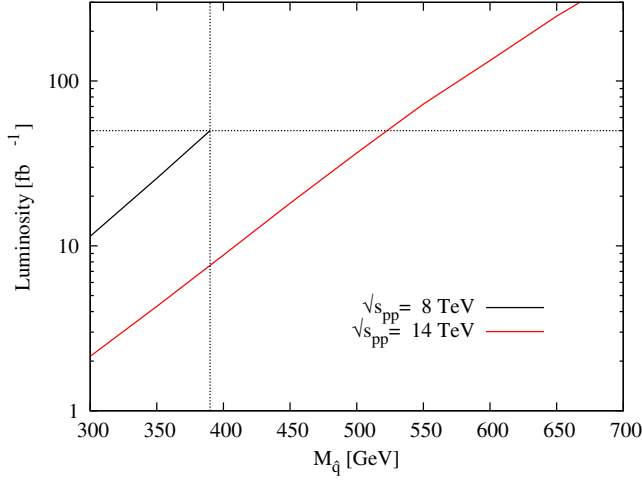


FIG. 7 (color online). Required luminosity for 5σ discovery is plotted as a function of $M_{\tilde{q}}$ for the LHC with center-of-mass energy 8 and 14 TeV.

2. Two jets + Z boson + W boson signature

Another interesting final state results from the pair production of mirror quarks which then decay to give $2\text{jets} + Z + W$ signal. This happens when one mirror quark decays into qZ while the other one decays into qW . As before we have considered the Z boson as a standard object without simulating its decay to leptons (electrons and muons). Even the W boson can be reconstructed to a certain efficiency in the leptonic channel, where the neutrino p_z is determined by using the W mass constraints. This is possible because of a single neutrino in the final state. However, we have chosen to ignore the W as a standard object since the qZ resonance will be much more well defined and with less ambiguity. In our parton-level Monte Carlo analysis,

TABLE VI. Acceptance cuts on the kinematical variables. p_T^l is the transverse momentum and η^l is the rapidity of the lepton. $\Delta R(l, j_{1,2})$ is the distance among the jet-lepton pairs in the η - ϕ plane, with ϕ being the azimuthal angle.

Kinematic variable	Minimum value	Maximum value
p_T^l	25 GeV	...
η^l	-2.5	2.5
$\Delta R(l, j_{1,2})$	0.4	...

we have simulated the decay of W bosons into leptons (electron and muons only) and neutrinos. Electrons and muons show charge tracks in the tracker and are detected at the electromagnetic calorimeter and muon detector, respectively. However, neutrinos remain invisible in the detector and give rise to an imbalance in the visible transverse momentum vector, which is known as missing transverse momentum (\cancel{p}_T). Therefore, the resulting signature in this case will be $2\text{jets} + 1\text{ charged lepton} + Z + \cancel{p}_T$.

The dominant SM background to the signal arises from the production of ZW pairs in association with two jets. Both signal and background jet energy are smeared by a Gaussian function defined in Eq. (23). To ensure the visibility of the jets at the detector, acceptance cuts listed in Table IV are applied on the jets. The acceptance cuts for the lepton are listed in Table VI. We do not apply any cuts on the missing transverse momentum. With these sets of cuts (A.C.) on jets (see Table IV) and lepton (see Table VI), we have computed the signal and background cross sections for the LHC with 8 and 14 TeV center-of-mass energy and presented them in Table VII. Table VII shows that for relatively large mirror quark masses, signal cross sections are much smaller than the SM background cross section. For example, at the LHC with 14 TeV center-of-mass

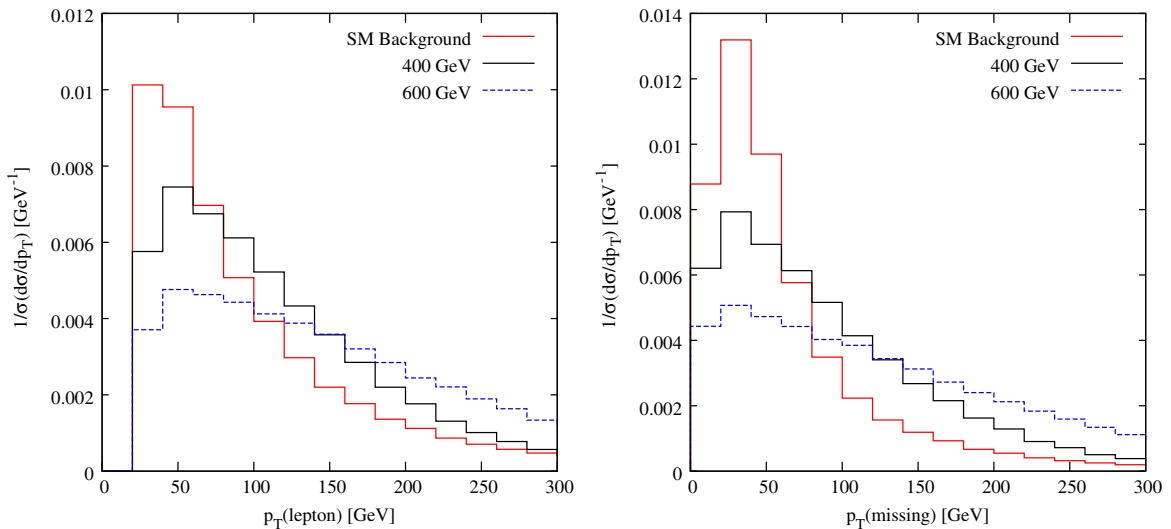


FIG. 8 (color online). Normalized lepton p_T (left panel) and missing p_T (right panel) distributions for the signal ($m_{\tilde{q}} = 400$ and 600 GeV) and the SM background after the acceptance cuts at the LHC with $\sqrt{s} = 14$ TeV.

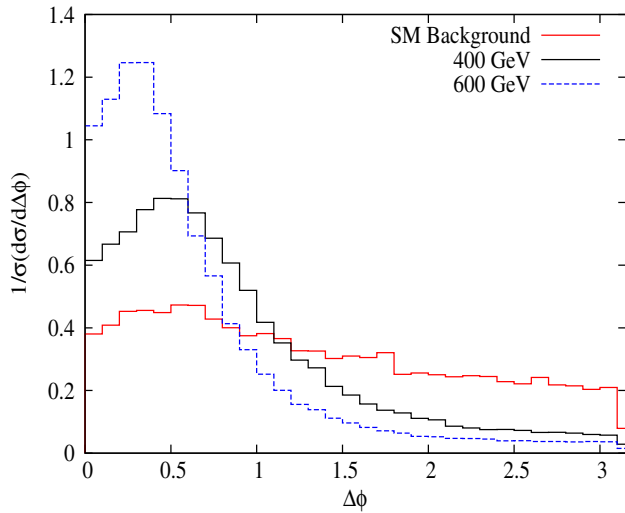


FIG. 9 (color online). Normalized azimuthal angle $\Delta\phi(\vec{p}_T^l, \vec{p}_T^{\text{miss}})$ distributions between lepton p_T vector and missing p_T vector after the acceptance cuts at the LHC with $\sqrt{s} = 14$ TeV. Signal distributions are presented for two different values of mirror quark mass ($m_{\hat{q}} = 400$ and 600 GeV).

energy, the signal-to-background ratio is 0.14 after acceptance cuts for $m_{\hat{q}} = 600$ GeV.

The signal contains a lepton, and \vec{p}_T arises from the decay of a W boson. The SM background lepton and \vec{p}_T also result from the W -boson decay. However, the signal W boson will be boosted in most of the events since it arises from the decay of a TeV-scale mirror quark. We have tried to exploit this feature of the signal for the further enhancement of signal-to-background ratio. We have examined the following kinematic distributions:

- (i) In Fig. 8, we have presented normalized lepton p_T (left panel) and missing p_T (right panel) distributions for the signal ($m_{\hat{q}} = 400$ and 600 GeV) and the SM background at the LHC with $\sqrt{s} = 14$ TeV. The boost of the signal W boson results in a long tail in the signal lepton and missing p_T distributions. Figure 8 shows that harder cuts on the lepton and/or missing p_T will suppress the SM background significantly. However, these cuts will also reduce signal cross sections considerably. For example, a kinematic requirement of $p_T > 75$ GeV on the

charged lepton at 14 TeV LHC will reduce 45% of the SM background and 25% of the signal for $m_{\hat{q}} = 600$ GeV. As a result, we do not use any further cuts on lepton and/or missing p_T .

- (ii) Since the signal W boson is boosted, we expect that the signal lepton and neutrino will be collimated. Therefore, it is viable to study the azimuthal angle ($\Delta\phi$) between lepton transverse momentum vector (\vec{p}_T^l) and missing transverse momentum vector (\vec{p}_T^{miss}). In Fig. 9, we have presented normalized $\Delta\phi(\vec{p}_T^l, \vec{p}_T^{\text{miss}})$ distributions for the signal ($m_{\hat{q}} = 400$ and 600 GeV) and the SM background at the LHC with $\sqrt{s} = 14$ TeV. Since the background W bosons are predominantly produced with small transverse momentum, background $\Delta\phi(\vec{p}_T^l, \vec{p}_T^{\text{miss}})$ distribution is almost flat (see Fig. 9), whereas the signal $\Delta\phi(\vec{p}_T^l, \vec{p}_T^{\text{miss}})$ distributions peak in the small $\Delta\phi(\vec{p}_T^l, \vec{p}_T^{\text{miss}})$ region. As a result, we have imposed an upper bound of 1 on the azimuthal angle between lepton p_T vector and missing p_T vector: $\Delta\phi(\vec{p}_T^l, \vec{p}_T^{\text{miss}}) < 1$. We collectively refer to acceptance cuts and $\Delta\phi(\vec{p}_T^l, \vec{p}_T^{\text{miss}}) < 1$ cut as Cut I. The signal and background cross sections after Cut I are presented in Table VII. For 14 TeV center-of-mass energy, $\Delta\phi(\vec{p}_T^l, \vec{p}_T^{\text{miss}}) < 1$ cut reduces 55% of the SM background and 14% of the signal for $m_{\hat{q}} = 600$ GeV and thus enhances the signal to background ratio by a factor of about 2.
- (iii) After $\hat{q}\hat{q}$ production, one mirror quark decays into qZ pair. Therefore, signal jet- Z invariant mass distribution is characterized by a peak at $m_{\hat{q}}$. After ordering the jets according to their p_T hardness ($p_T^{j_1} > p_T^{j_2}$), we have constructed the following two invariant masses: (i) M_1 is the invariant mass of the j_1 - Z pair, and (ii) M_2 is the invariant mass of the j_2 - Z pair. The signal and background invariant mass distributions are presented in Fig. 10 for the LHC with $\sqrt{s} = 14$ TeV. For the further enhancement of the signal-to-background ratio, we have imposed cuts on M_2 in a way similar to that discussed in the previous section. This cut and Cut I

TABLE VII. Signal and SM background cross-section after the acceptance cuts (A.C.), Cut I and Cut II for two different values of proton-proton center-of-mass energies. Signal cross sections (σ_{Signal}) are presented for three different values of mirror quark masses ($M_{\hat{q}}$).

$M_{\hat{q}}$ GeV	$\sqrt{s} = 8$ TeV						$\sqrt{s} = 14$ TeV						
	Signal			Background			Signal			Background			
	A.C.	Cut I	Cut II	A.C.	Cut I	Cut II	$M_{\hat{q}}$ GeV	A.C.	Cut I	Cut II	A.C.	Cut I	Cut II
300	14.4	7.28	3.13			0.74	400	26.3	18.1	6.46			2.13
350	8.01	4.85	1.92	6.69	2.81	0.63	500	9.36	7.33	2.39	26.4	11.9	1.39
400	4.35	2.98	1.11			0.51	600	3.6	3.07	0.95			0.90

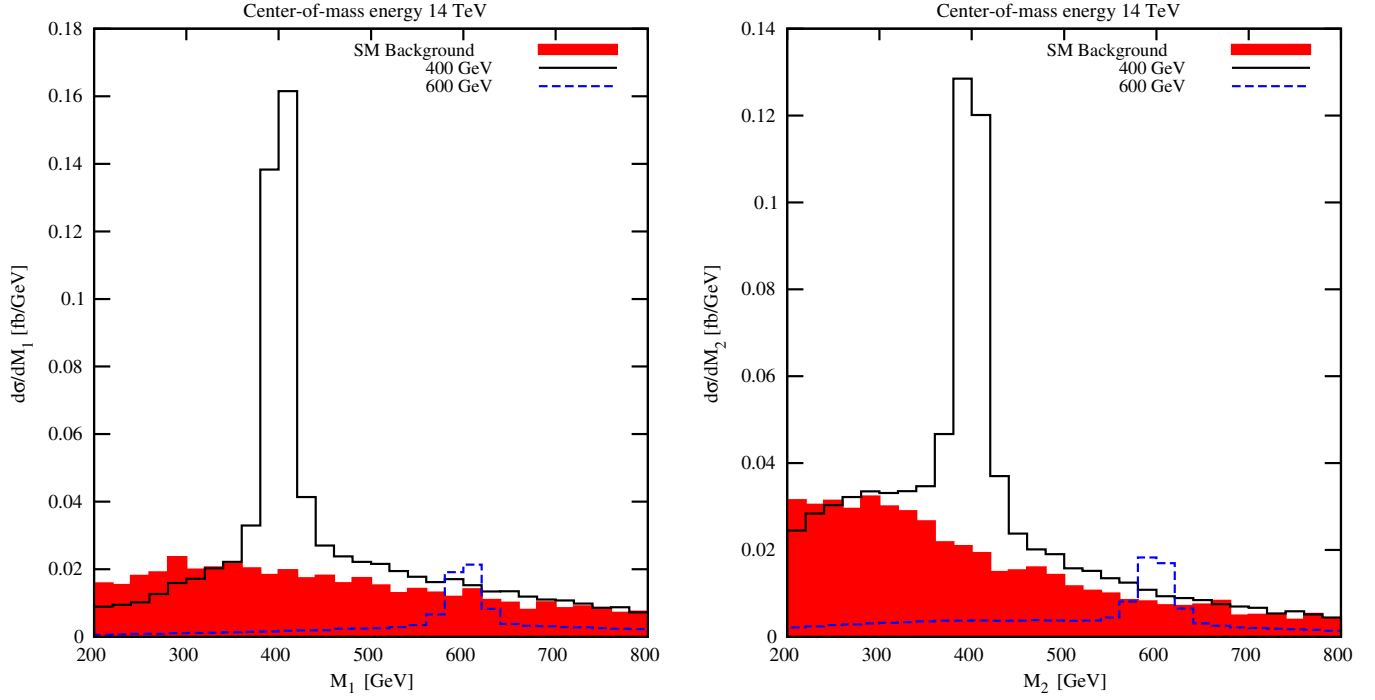


FIG. 10 (color online). Jet-Z invariant mass distributions after Cut I for the signal ($m_{\hat{q}} = 400$ and 600 GeV) and the SM background at the LHC with 14 TeV center-of-mass energy.

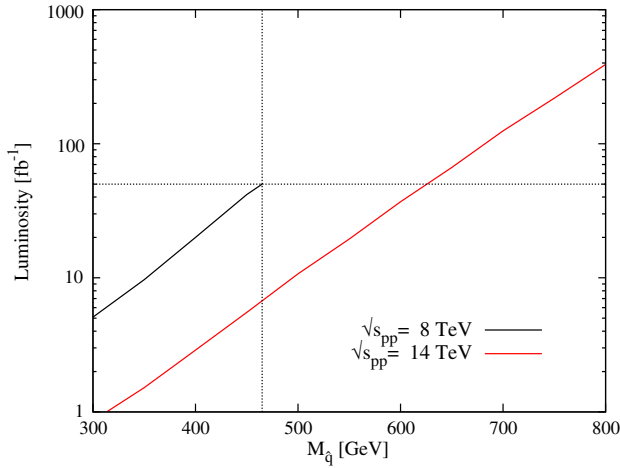


FIG. 11 (color online). Required luminosity for 5σ discovery in two-jets + one lepton + one Z boson + \cancel{p}_T channel is plotted as a function of $M_{\hat{q}}$ for the LHC with center-of-mass energy 8 and 14 TeV.

are collectively referred to as Cut II in Table VII. Table VII shows that for $m_{\hat{q}} = 600$ GeV, the j_2 - Z invariant mass cut suppresses the SM background by a factor of about 13, whereas the signal is reduced by a factor of only 3.

To estimate the required integrated luminosity for the discovery of the mirror quarks in two jets + one charged lepton + Z + \cancel{p}_T channel, we have used Eq. (25). The signal and background cross sections after

Cut II in Table VII show that at the LHC with center-of-mass energy 8 (14 TeV), 400 (600 GeV) mirror quark mass can be probed with integrated luminosity 20 (37 fb^{-1}). In Fig. 11, we have presented the required luminosity for 99.4% C.L. discovery in two jets + one charged lepton + Z + \cancel{p}_T channel as a function of $M_{\hat{q}}$ for the LHC with center-of-mass energy 8 and 14 TeV.

IV. SUMMARY AND CONCLUSIONS

In this work, we have a realistic left-right symmetric model with mirror fermions and mirror Higgs and the possibility of discovering the low-lying mirror fermions at the LHC. The model is $SU(3)_C \otimes SU(2)_L \otimes SU(2)_R \otimes U(1)'_Y$, supplemented by a discrete Z_2 . For each chiral multiplet of the SM fermions, we have corresponding mirror fermions of opposite chirality. The symmetry is broken to the usual SM symmetry by a mirror Higgs doublet. The mixing between the SM fermions and the mirror fermions is achieved by using a Higgs multiplet, which is a singlet under the gauge symmetry but odd under the Z_2 symmetry. The model has singlet right-handed neutrinos, and the corresponding mirror neutrinos that are even under Z_2 . These are used to generate tiny neutrino masses $\approx 10^{-11}$ GeV with a primary symmetry-breaking scale of $\approx 10^7$ GeV (which is the VEV of the mirror Higgs doublet). In this model, only the mirror fermion of the first family ($\hat{e}, \hat{u}, \hat{d}$) are light with well-defined relative spectrum. All the other mirror fermions are much heavier and well above the LHC reach. Since the model is completely

left-right symmetric in the fermion sector, it is naturally anomaly free. Parity conservation and the nature of the fermion mass matrices also provide a solution for the strong CP in the model.

The light mirror fermions, \hat{u} , \hat{d} , with masses around a few hundred GeV to about 1 TeV, can be pair produced at the LHC via their QCD color interactions. They dominantly decay to a Z boson plus the corresponding ordinary fermion ($\hat{u} \rightarrow u + Z$, $\hat{d} \rightarrow d + Z$) or to a W boson and the corresponding ordinary fermions ($\hat{u} \rightarrow d + W$, $\hat{d} \rightarrow u + W$). (The decays ($\hat{u} \rightarrow u + H$, $\hat{d} \rightarrow d + H$) are highly suppressed for most of the parameter space). Thus the most striking signal of the model is the existence of resonances in the jet plus Z channel. Since both the jet and the Z are coming from the decay of a very heavy particle, both will have very high p_T . We have shown that putting a high p_T cut on the jet, and reconstructing the Z in the e^+e^- or $\mu^+\mu^-$ channels, these resonances \hat{u} , \hat{d} can be reconstructed up to a mass of ≈ 350 GeV at the 8 TeV LHC and up to a mass of ≈ 550 GeV at the 14 TeV LHC. We are not aware of any other model that predicts such a resonance. We have also studied, in some detail, the final states arising from the pair productions of these light mirror fermions at the LHC. These final states are $(uZ)(\bar{u}Z)$, $(dZ)(\bar{d}Z)$, $(uZ)(\bar{d}W)$, $(dZ)(\bar{u}W)$, and the subsequent decays of W and Z into the leptonic channels. The signals are much more observable in the (jet jet ZZ) channel than the (jet jet ZW) channel because of the missing neutrino in the latter. (The resonance in the signals involving the two W 's will be difficult to observe). We have studied these final

states and the corresponding backgrounds and find that the reaches for the light mirror quarks can be ≈ 450 GeV at the 8 TeV LHC with luminosity of 30 fb^{-1} and up to 750 GeV at the 14 TeV LHC with 300 fb^{-1} luminosity.

Our model predicts a definite pattern of spectrum for the light mirror fermions, \hat{e} , \hat{u} , \hat{d} . Thus with $m_{\hat{u}} < m_{\hat{d}}$, if a resonance \hat{u} is observed, we expect a nearby \hat{d} within a few hundred GeV. This makes the prediction of the model somewhat unique. Also the \hat{e} will have even lower mass and can be looked for in the proposed future e^+e^- collider.

In this paper, we have studied the collider phenomenology of TeV-scale mirror fermions in the framework of a particular variant of LRMM in which mirror fermions dominantly decay into the SM fermion and W or Z boson. However, our collider analysis is general enough to be applicable to a class of models with TeV-scale fermions, such as chiral fourth-generation extensions or models with vectorlike fermions decaying into a SM fermion and W or Z boson.

ACKNOWLEDGMENTS

The work of S. C., K. G. and S. N. is supported by the U.S. Department of Energy, Grant No. DE-FG02-04ER41306. The work of S. K. R. was partially supported by funding available from the Department of Atomic Energy, Government of India, for the Regional Centre for Accelerator-based Particle Physics, Harish-Chandra Research Institute.

-
- [1] J. C. Pati and A. Salam, *Phys. Rev. D* **10**, 275 (1974); R. N. Mohapatra and J. C. Pati, *Phys. Rev. D* **11**, 566 (1975); G. Senjanovic and R. N. Mohapatra, *Phys. Rev. D* **12**, 1502 (1975); R. N. Mohapatra and R. E. Marshak, *Phys. Lett.* **91B**, 222 (1980); R. N. Mohapatra, *Unification and Supersymmetry. Graduate Texts in Contemporary Physics* (Springer-Verlag, Berlin, 1992), 2nd ed..
- [2] H. Georgi, *AIP Conf. Proc.* **23**, 575 (1975); H. Fritzsch and P. Minkowski, *Ann. Phys. (N.Y.)* **93**, 193 (1975).
- [3] F. Gursey and M. Serdaroglu, *Nuovo Cimento A* **65**, 337 (1981); Y. Achiman and B. Stech, *Phys. Lett.* **77B**, 389 (1978).
- [4] P. Candelas, G. T. Horowitz, A. Strominger, and E. Witten, *Nucl. Phys.* **B258**, 46 (1985).
- [5] D. Chang, R. N. Mohapatra, and M. K. Parida, *Phys. Rev. D* **30**, 1052 (1984).
- [6] C. S. Aulakh, K. Benakli, and G. Senjanovic, *Phys. Rev. Lett.* **79**, 2188 (1997); C. S. Aulakh, A. Melfo, A. Rasin, and G. Senjanovic, *Phys. Rev. D* **58**, 115007 (1998).
- [7] E. K. Akhmedov, M. Lindner, E. Schnapka, and J. W. F. Valle, *Phys. Rev. D* **53**, 2752 (1996); Z. Chacko, H.-S. Goh, and R. Harnik, *J. High Energy Phys.* **01** (2006) 108.
- [8] T.-j. Li, F. Wang, and J. M. Yang, *Nucl. Phys.* **B820**, 534 (2009); C. Balazs, T.-j. Li, F. Wang, and J. M. Yang, *J. High Energy Phys.* **09** (2009) 015; C. Balazs, T. Li, F. Wang, and J. M. Yang, *J. High Energy Phys.* **01** (2011) 023.
- [9] T. D. Lee and C.-N. Yang, *Phys. Rev.* **104**, 254 (1956).
- [10] Z. K. Silagadze, *Yad. Fiz.* **60N2**, 336 (1997) [*Phys. At. Nucl.* **60**, 272 (1997)].
- [11] R. Foot and R. R. Volkas, *Phys. Rev. D* **52**, 6595 (1995).
- [12] Z. G. Berezhiani and R. N. Mohapatra, *Phys. Rev. D* **52**, 6607 (1995).
- [13] K. S. Babu and R. N. Mohapatra, *Phys. Rev. D* **41**, 1286 (1990);
- [14] K. S. Babu and R. N. Mohapatra, *Phys. Rev. Lett.* **62**, 1079 (1989); S. M. Barr, D. Chang, and G. Senjanovic, *Phys. Rev. Lett.* **67**, 2765 (1991); P. H. Gu, *Phys. Lett. B* **713**, 485 (2012).
- [15] J. Maalampi and M. Roos, *Phys. Rep.* **186**, 53 (1990).
- [16] V. E. Ceron, U. Cotti, J. L. Diaz-Cruz and M. Maya, *Phys. Rev. D* **57**, 1934 (1998); S. Dawson, E. Furlan, and I. Lewis, *Phys. Rev. D* **87**, 014007 (2013).
- [17] P. Q. Hung, *Phys. Lett. B* **649**, 275 (2007).
- [18] B. Aubert *et al.* (BABAR Collaboration), *Phys. Rev. Lett.* **95**, 041802 (2005).

- [19] K. Hayasaka *et al.* (Belle Collaboration), *Phys. Lett. B* **666**, 16 (2008).
- [20] P. Q. Hung, *Phys. Lett. B* **659**, 585 (2008).
- [21] V. Barger and R. Phillips, *Collider Physics* (Westview Press, New York, 1996).
- [22] J. Pumplin, D. R. Stump, J. Huston, H. L. Lai, P. M. Nadolsky, and W. K. Tung, *J. High Energy Phys.* **07** (2002) 012.
- [23] M. Cacciari, S. Frixione, M. L. Mangano, P. Nason, and G. Ridolfi, *J. High Energy Phys.* **09** (2008) 127.
- [24] H. Baer, M. Bisset, C. Kao, and X. Tata, *Phys. Rev. D* **46**, 1067 (1992).
- [25] *Handbook of Mathematical Functions with Formulas, Graphs and Mathematical Tables*, edited by M. Abramowitz and A. Stegun (Dover, New York, 1965).